Structure and phase transitions in the ferroelastic $[C(NH_2)_3]_3Bi_2Br_9$ crystal

1999 J. Phys.: Condens. Matter 11 4731

(http://iopscience.iop.org/0953-8984/11/24/314)

J. Phys.: Condens. Matter **11** (1999) 4731–4746. Printed in the UK PII: S0953-8984(99)00381-1

Structure and phase transitions in the ferroelastic $[C(NH_2)_3]_3Bi_2Br_9$ crystal

R Jakubas†, J Zaleski‡, B Kosturek§ and G Bator†

† Faculty of Chemistry, University of Wrocław, F Joliot Curie 14, 50-383 Wrocław, Poland
‡ Institute of Chemistry, University of Opole, 45-052 Opole, Poland
§ Institute of Experimental Physics, University of Wrocław, 9 Max Born Square, 50-204 Wrocław, Poland

Received 23 December 1998, in final form 8 April 1999

Abstract. Differential scanning calorimetry, dilatometric, dielectric and linear birefringence measurements have been used to study the ferroelastic $[C(NH_2)_3]_3Bi_2Br_9$ crystal. The x-ray studies showed that it crystallizes at room temperature in the monoclinic symmetry, space group $P2_1/m$. The crystal undergoes a complex sequence of phase transitions: at 311 K, 333.5 K, 350 K, 415 K and 425 K. All phase transitions were found to be of first order type. The ferroelastic domain structure is maintained from room temperature up to 425 K. The temperature measurements of the linear birefringence and optical observations suggest the tetragonal symmetry of the parent paraelastic phase above 425 K.

1. Introduction

Alkylammonium halogenoantimonates(III) and bismuthates(III) of the general formula $[NH_{4-n}(CH_3)_n]_3Me_2X_9$ (Me = Sb, Bi, X = Cl, Br, I, n = 1–4) exhibit an interesting order–disorder structural phase transition [1–6]. It was shown that the dynamic of organic cations in these crystals significantly changes at the phase transition temperatures, pointing out their important role in the mechanism of transitions. Depending on the size of organic cations as well as the halogen atoms, ordering of cations may occur, giving rise to different structural characteristics and to various physical properties. The anionic $Me_2X_9^{3-}$ sublattice may be built of: (i) polyanionic one-dimensional zigzag chains (methylammonium chloride analogues), (ii) two-dimensional layers (present in dimethylammonium and trimethylammonium salts), (iii) isolated bioctahedral anionic units (various alkylammonium iodoantimonates and bismuthates). The second group of crystals (ii) shows considerable importance because of their physical properties such as pyro- and ferroelectricity and non-linear electrooptic effects. Much work has been devoted to the ferroelectric properties occurring in many salts of this subgroup: $(CH_3NH_3)_3Bi_2Br_9$ [7], $[(CH_3)_2NH_2]_3Sb_2X_9$ [8, 9], $[(CH_3)_3NH]_3Sb_2Cl_9$ [10]. The ferroelasticity has been discovered in the methylammonium and dimethylammonium analogues; $(CH_3NH_3)_3Sb_2Br_9$ [11], $(CH_3NH_3)_3Bi_2Br_9$ [12], $[(CH_3)_2NH_2]_3Sb_2Br_9$ [13], $[(CH_3)_2NH_2]_3Sb_2Cl_9$ [14] and $[(CH_3)_2NH_2]_3Bi_2I_9$ [15]. The Brillouin study of the phase transitions in $(CH_3NH_3)_3Sb_2Br_9$ [16] and $(CH_3NH_3)_3Bi_2Br_9$ [17] have shown that the ferroelasticity is driven by an order–disorder relaxation mode.

0953-8984/99/244731+16$19.50

In searching for new ferroelastic or ferroelectric halogenoantimonates(III) and bismuthates(III) crystals the guanidinium analogue $[C(NH_2)_3]_3Bi_2Br_9$ (abbreviated as GBB) was synthesized. This paper describes the study of the structural phase transitions occurring in new ferroelastic GBB crystals using x-ray diffraction, differential scanning calorimetry, dilatometric, dielectric, birefringence and optical measurements.

2. Experimental details

The crystals of $[C(NH_2)_3]_3Bi_2Br_9$ were synthesized by reaction of $[C(NH_2)_3]_2CO_3$ and $BiBr_3$ in concentrated hydrobromic acid. Large single crystals were grown by a slow evaporation at constant room temperature. The stoichiometry was confirmed by elemental analysis.

Differential scanning calorimetry (DSC) measurements were carried out using a Perkin–Elmer DSC-7 calorimeter. The DSC measurements were performed with the cooling/heating rates ranging from 3 to 20 K min^{-1}.

The linear thermal expansion was measured using a thermomechanical analyser (Perkin–Elmer TMA-7). The samples used in the measurements were prepared in the form of thin plates of dimensions $7 \times 7 \times 1$ mm^3 (natural plates). The anomalies in the vicinity of phase transitions were reproducible within 20% for each sample. The accuracy of the thermal expansion determination was about 5%. The dilatometric measurements were performed during heating and cooling runs at a rate of 1.5 K min^{-1}.

The complex electric permittivity, ε^* was measured using an HP 4285 *LCR* meter between 75 kHz and 30 MHz in the temperature range 300 K–450 K with a cooling/heating rate of 0.2 K min^{-1} in the vicinity of the phase transitions and 1 K elsewhere. Plates with the typical dimensions of $5 \times 5 \times 1$ mm^3 along the *b* axis were prepared for the dielectric measurements and gold electrodes were applied to their large faces. The overall error for the real and imaginary part of the complex electric permittivity was less than 5%.

The optical methods applied to the detection of the phase transitions and the description of the resulting phases were: polarized microscopy observations monitored by CCD camera, measurements of the absolute value of the linear birefringence and determination of the optical indicatrix position inside ferroelastic domains using the Ehringhaus compensator. The temperature dependence of the linear birefringence was studied using the rotating analyser method [18]. A 1 mW He–Ne laser served as a light source ($\lambda = 632.8$ nm). Measurements of the absolute value of the birefringence were less accurate due to large optical dispersion of the crystal [19]. The accuracy achieved for the birefringence change measurements was 10^{-6}. The cooling and heating rates were 0.5 K min^{-1} (0.2 K min^{-1} in the phase transition regions).

Data for structure determination was collected on a KM-4 KUMA diffractometer with Mo Kα radiation ($\lambda = 0.710\,73$ Å, graphite monochromator) and Oxford Cryosystem cooler enabling temperature changes between 78 and 370 K. Lattice parameters were refined from setting angles of 23 reflections in the $14 < 2\theta < 24^\circ$ range. Data of experimental conditions are presented in table 1.

A total of 1864 reflections with $4^\circ < 2\theta < 46^\circ$ were collected using the ω–θ scan technique (scan speed 0.02–0.15° s^{-1}); scan width 1.33°. Two control reflections measured after an interval of 50 reflections show that the intensity variation was negligible. Lorentz, polarization and semiempirical absorption corrections were applied.

Scattering factors for neutral atoms and corrections for anomalous dispersion were as in the SHELX97 program system [20]. The SHELX97 program was used for all the structure calculations while SHELXTL PC for drawings. A list of the calculated and observed structure factors may be obtained from authors on request.

Table 1. Crystal data and structure refinement for GBB.

Identification code	GBB
Empirical formula	$(C(NH_2)_3)_3Bi_2Br_9$
Formula weight	1317.4
Temperature	293(2) K
Wavelength	0.710 73 Å
Crystal system, space group	Monoclinic, $P2_1/m$
Unit cell dimensions	$a = 7.834(2)$ Å
	$b = 20.176(4)$ Å $\beta = 97.54(3)^\circ$
	$c = 8.463(2)$ Å
Volume	1326.1(5) Å^3
Z, calculated density	2, 3.299 mg m^{-3}
Absorption coefficient	26.819 mm^{-1}
$F(000)$	1160
Crystal size	$0.2 \times 0.3 \times 0.35$ mm^3
θ range for data collection	2° to 23°
Index ranges	$-8 \leqslant h \leqslant 8$, $-21 \leqslant k \leqslant 0$, $0 \leqslant l \leqslant 9$
Reflections collected/unique	1864/1751 [$R_{int} = 0.047$]
Completeness to $\theta = 23$	89.8%
Refinement method	Full-matrix least squares on F^2
Data/restraints/parameters	1751/0/115
Goodness of fit on F^2	1.031
Final R indices [$I > 2\sigma(I)$]	$R_1 = 0.047$, $wR_2 = 0.123$
R indices (all data)	$R_1 = 0.113$, $wR_2 = 0.144$
Largest difference peak and hole	1.510 and -1.464 e Å^{-3}

Symmetries of high temperature phases were determined by x-ray diffraction from setting angles of 20–28 reflections in the $14 < 2\theta < 30^\circ$ range. Space groups of phases IV and III were determined by collecting data sets at 345 K and 355 K and the evaluation of systematic absences.

3. Results and discussion

3.1. X-ray studies

The atomic coordinations and selected bond lengths are given in tables 2 and 3. The anionic sublattice of GBB consists of isolated bioctahedral $Bi_2Br_9^{3-}$ units composed of two face sharing $BiBr_6^{3-}$ octahedra. There are three bridging and three terminal bromines in each of them. Bi–Br bond lengths fall in two clearly defined ranges 2.690(3)–2.712(3) Å for terminal bromines and 3.039(3)–3.053(2) Å for bridging ones. Br–Sb–Br *cis* to each other bond angles fall in the range 79.7(1)–97.4(1)$^\circ$ and are much distorted from the ideal value of 90°. There are two crystallographically inequivalent guanidinium cations in the crystal structure. The organic cations are ordered. They are connected to bromine ions by relatively weak N–H. . . Br hydrogen bonds. A view of the unit cell is presented in figure 1.

To determine symmetries of high temperature phases of GBB we increased temperature stepwise and refined lattice parameters in phases VI, V, IV and III. In phase V we observed additional reflections, which could not be assigned integer indices along the *b* direction. This may suggest the presence of modulated structure with modulation vector along the *b* direction. At T_{c4} the modulation vanishes and systematic absences show that symmetry in the phase IV is again $P2_1/m$ ($a = 7.874(8)$, $b = 20.341(10)$, $c = 8.466(6)$ Å, $\beta = 98.37(3)^\circ$ at 345 K).

Table 2. Atomic co-ordinates ($\times 10^4$) and equivalent isotropic displacement parameters (Å$^2 \times 10^3$) for GBB. U_{eq} is defined as one third of the trace of the orthogonalized U_{ij} tensor.

	x	y	z	U_{eq}
Bi(1)	2311(1)	1513(1)	1516(1)	33(1)
Br(1)	3315(4)	2500	4187(3)	36(1)
Br(2)	3946(4)	2500	−543(4)	50(1)
Br(3)	1462(3)	709(1)	−1031(3)	54(1)
Br(4)	5363(3)	882(1)	2297(3)	56(1)
Br(5)	667(4)	818(1)	3571(3)	63(1)
Br(6)	−640(4)	2500	785(3)	41(1)
C(1)	3630(3)	−886(13)	2890(3)	52(7)
N(1)	2450(3)	−833(13)	3870(2)	73(8)
N(2)	5210(3)	−954(13)	3440(2)	75(8)
N(3)	3210(3)	−774(11)	1330(3)	67(7)
C(2)	−1620(5)	2500	−3930(3)	40(9)
N(4)	−2220(4)	2500	−5560(3)	52(8)
N(5)	−2840(3)	2500	−2990(3)	52(8)
N(6)	−10(3)	2500	−3440(4)	95(15)

Table 3. Selected bond lengths [Å] and angles [°] for GBB.

Bi(1)–Br(1)	3.039(2)
Bi(1)–Br(2)	3.039(3)
Bi(1)–Br(3)	2.709(2)
Bi(1)–Br(4)	2.712(3)
Bi(1)–Br(5)	2.690(3)
Bi(1)–Br(6)	3.053(2)
Br(1)–Bi(1)–Br(2)	84.8(1)
Br(1)–Bi(1)–Br(3)	175.5(1)
Br(1)–Bi(1)–Br(4)	89.6(1)
Br(1)–Bi(1)–Br(5)	87.7(1)
Br(1)–Bi(1)–Br(6)	80.7(1)
Br(2)–Bi(1)–Br(3)	90.8(1)
Br(2)–Bi(1)–Br(4)	91.3(1)
Br(2)–Bi(1)–Br(5)	170.4(1)
Br(2)–Bi(1)–Br(6)	79.7(1)
Br(3)–Bi(1)–Br(4)	91.7(1)
Br(3)–Bi(1)–Br(5)	96.6(1)
Br(3)–Bi(1)–Br(6)	97.4(1)
Br(4)–Bi(1)–Br(5)	94.6(1)
Br(4)–Bi(1)–Br(6)	167.2(1)
Br(5)–Bi(1)–Br(6)	93.3(1)
Bi(1)–Br(1)–Bi(1)#1	82.0(1)
Bi(1)#1–Br(6)–Bi(1)	81.5(1)

Symmetry transformations used to generate equivalent atoms: #1$x, -y + 1/2, z$.

Between 273 K and 345 K we observed almost no increase of the lattice parameter c with largest changes of the b parameter. A significant change of the beta angle between 293 and 345 K should be noted.

Transformation to phase III leads to the change of the symmetry from monoclinic to the orthorhombic $Cmcm$ phase with $a = 10.657(4)$, $b = 12.564(5)$, $c = 20.323(7)$ Å at 355 K. This phase transition leads to the twofold increase of the volume of the unit cell with resultant

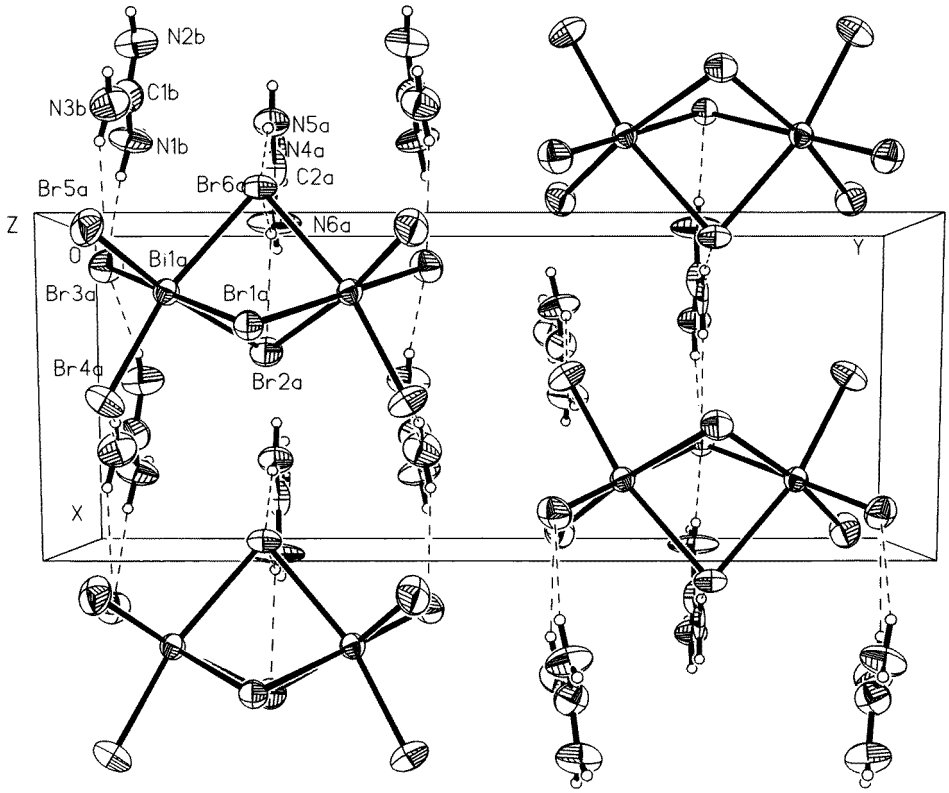

Figure 1. Projection of the crystal structure of $[C(NH_2)_3]_3Bi_2Br_9$ on the *a*–*b*-plane at 293 K. Thermal ellipsoids at 50% probability.

a and *b* parameters of the orthorhombic phase oriented at ∼45° to the *a* and *c* parameters of the initial monoclinic phase.

3.2. Differential scanning calorimetry measurements

Three thermal anomalies were detected in the temperature range 280–360 K during the first and second DSC scans (see figure 2). We should notice the splitting of two peaks at 333.5 and 350 K (on heating). These effects are reversible and additionally a needle-like structure of the DSC curve is observed. It may be connected with the changes in the ferroelastic domains structure. Such a sequence of phase transitions (three heat anomalies) is observed if the crystal is not heated above 410 K. The DSC curves in a wide temperature range between 280 and 450 K are shown in figure 3. At high temperature the GBB crystals exhibit two closely lying phase transitions at 415 and 425 K of first order type (run 3). It is interesting to note that in the cooling runs the sequence of phase transitions differs from that observed on heating if the crystal reaches 425 K (compare the runs 2 and 4). During the cooling run 4 instead of three phase transitions below 350 K only one, strong heat anomaly at 325 K is observed. During the next heating (run 5) of the sample, which had experienced the phase transitions at 415 and 425 K, only one peak at about 330 K is now visible. Such behaviour of DSC scans is observed for samples prepared as a single crystal. If the original sample is powdered no heat anomalies are visible during the first and second run between 290 and 360 K. The DSC curves exhibit

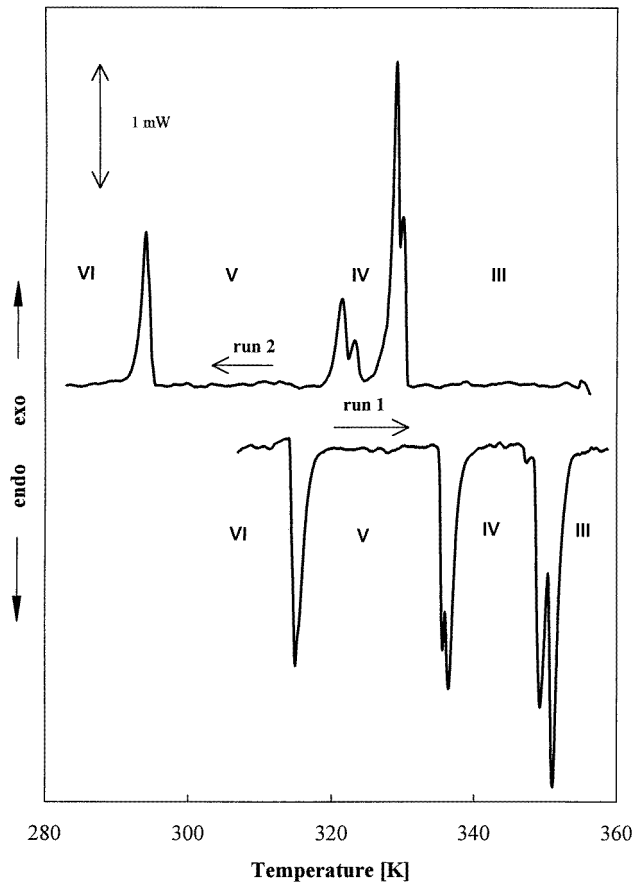

Figure 2. DSC curve of the $[C(NH_2)_3]_3Bi_2Br_9$ crystals between 280 and 360 K recorded on heating and cooling (sample mass 17.9 mg, scanning rate 5 K min^{-1}, sample not powdered).

only strong needle-like structure. Powdering of the sample does not influence the shape of heat anomalies at 415 and 425 K. Results of the calorimetric studies are collected in table 4. The thermal hysteresis was estimated from the scans performed at various rates extrapolated to a scanning rate of 0 K min^{-1}. The six crystalline phases of GBB are denoted successively as I, II, III, IV, V and VI starting from the phase existing above 425 K. Strong heat anomalies and large hysteresis phenomena indicate the first order character of all phase transitions. The estimated values of the transition entropies for the (IV $\rightarrow$ III), (III $\rightarrow$ II) and (II $\rightarrow$ I) transformations point out the order–disorder mechanisms. For the (IV $\rightarrow$ V) and (V $\rightarrow$ VI) transitions ΔS-values are lower than $R \ln 2$, which may suggest a possible disordering of the phases existing above 311 K.

3.3. Linear thermal expansion measurements

The overall behaviour of the thermal dilation of GBB single crystals along the *b*-axis is shown in figure 4. This direction is perpendicular to the large natural plates forming the cleavage plane *ac* of single crystals. During heating, the phase transitions at T_{c3} and T_{c5} are hardly visible, whereas the one at T_{c4} is seen as a small jump in $\Delta L/L_0$. The following two phase

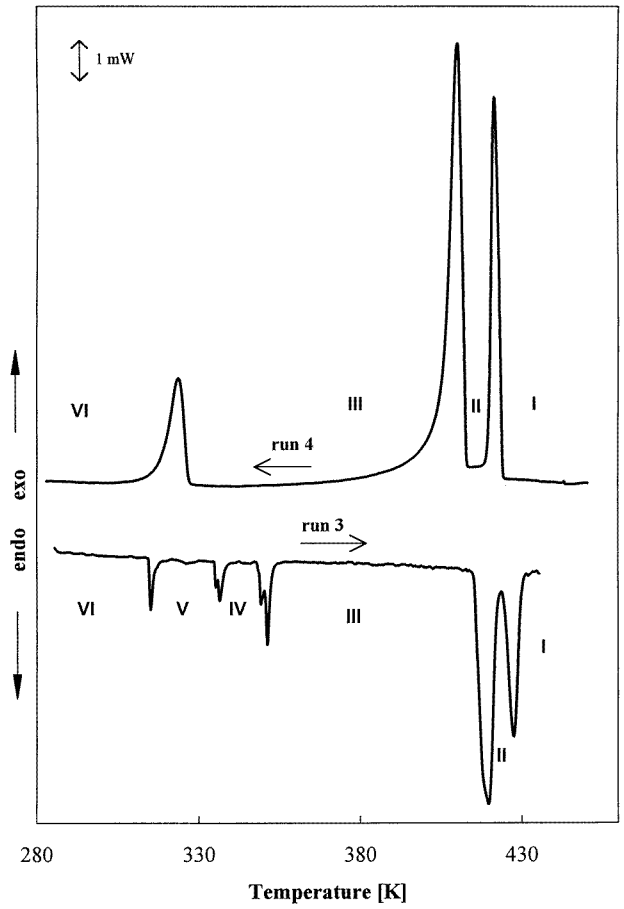

Figure 3. DSC curve of the $[C(NH_2)_3]_3Bi_2Br_9$ crystals between 280 and 450 K recorded on heating and cooling (sample mass 17.9 mg, scanning rate 5 K min^{-1}, sample not powdered).

Table 4. The transition temperatures, thermal hysteresis, enthalpy and entropy values of the phase transitions in GBB. The results were taken from DSC measurements (on heating).

Phase transition	T_c (K)	ΔT (K)	ΔH (kJ mol^{-1})	ΔS (J mol^{-1} K^{-1})
(VI → V)	311	14.5	4.0	3.0 (R ln 1.43)
(V → IV)	333.5	9	3.4	2.6 (R ln 1.37)
(IV → III)	350	4.6	6.1	4.6 (R ln 2.07)
(III → II)	415	2	34.2	26.0 (R ln 22.8)
(II → I)	425	1	14.5	11.0 (R ln 3.75)

transitions at T_{c2} and T_{c1} are accompanied by drastic change in dilation of the crystal of the order of 10%. Because of formation of the cracks in the sample at these two phase transitions the observed thermal anomalies are regarded only qualitatively. During cooling, the high temperature transitions are poorly reproducible. It is seen that the total effect in dilation is now of the order of 3%. The expected transition at 329 K is practically invisible, because of the strong deformation of the sample. The measurements were performed along the a- and c-directions. The results of dilatometric measurements along the a- and c-directions are

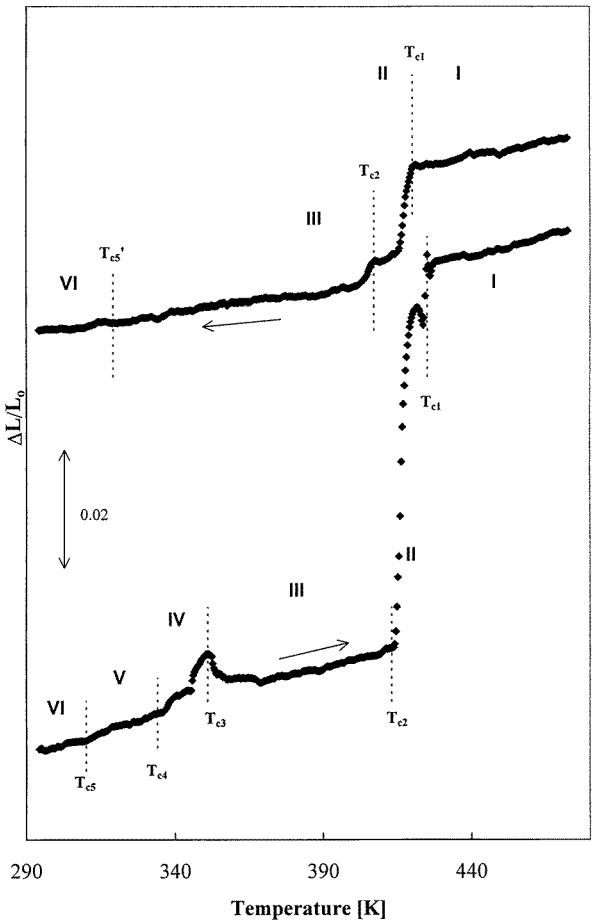

Figure 4. Temperature dependence of the linear thermal expansion, $\Delta L/L_0$, measured along the *b*-axis on cooling and heating at a rate of 1 K min^{-1} for $[C(NH_2)_3]_3Bi_2Br_9$.

displayed in figures 5 and 6. The phase transitions in the low temperature region are weak but clearly visible, whereas the ones at T_{c1} and T_{c2} are accompanied by a larger jump in the dilation (20% for the *a*-direction and 14% for the *c*). The measurements along the *a*- or *c*-directions confirmed the presence of the transition at 320 K. Comparing the DSC and dilatometric results one can state that sequence of the phase transitions is consistent.

3.4. Dielectric measurements

The real part of the complex electric permittivity (ε') in the temperature region 295–350 K between 500 kHz and 7 MHz along the *b*-direction during cooling (upper part) and heating (lower part) is shown in figure 7. For this sample we did not increase temperature above 350 K. The three phase transitions recorded in the low temperature region by DSC and dilatometric techniques are well evidenced by the dielectric method. The dielectric anomalies accompanying these phase transitions are well reproducible. Sharp discontinuities of the electric permittivity at T_{c3}, T_{c4} and T_{c5} are indicative of the first order transitions. The values of the electric permittivity over the low temperature phase transition region are quite small;

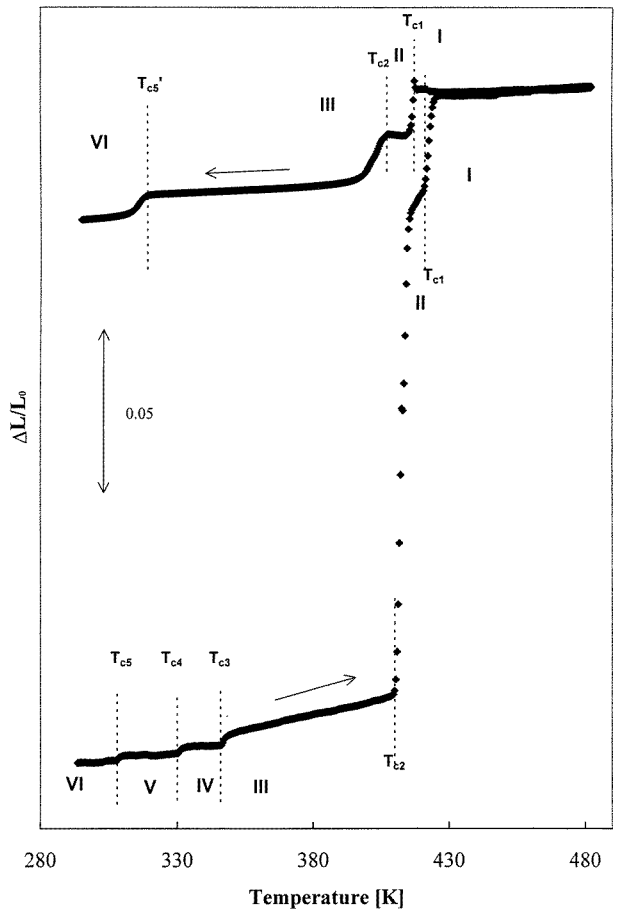

Figure 5. Temperature dependence of the linear thermal expansion, $\Delta L/L_0$, measured along the a-axis on cooling and heating at a rate of 1 K min^{-1} for $[C(NH_2)_3]_3Bi_2Br_9$.

the dielectric anomalies are rather subtle. The apparent transition temperature is almost independent of measuring frequency in the range from 75 kHz to 30 MHz. No dielectric dispersion is visible up to 350 K. The dielectric response of the sample which experienced the high temperature phase transitions, on cooling (ε'—upper part and ε''—lower part) is displayed in figure 8. The divergence of the electric permittivity is clearly visible above 390 K. It probably originates from the crystal defects and does not exhibit the features of the Debye-like dispersion. We should remember that the single crystals are destroyed during heating of the sample above 415 K. It is interesting (see figure 8) that the shape of ε'_b around the 330 K phase transition resembles the dielectric anomaly at T_{c3} during the heating run (figure 7). This may suggest that the phase transition observed on cooling at T_{c5} corresponds to the III $\rightarrow$ IV one recorded on heating.

Results of DSC, dielectric and x-ray studies allow us to suggest a probable mechanism of the phase transitions in GBB. It is well known that guanidinium cations have D_{3h} symmetry. On increasing temperature one can expect the onset of the C_3 type of reorientation of cations in the solid state. Probably such a type of motion is triggered at the phase transitions. The C_3 type reorientation, however, does not lead to the change of resultant dipole moment of the

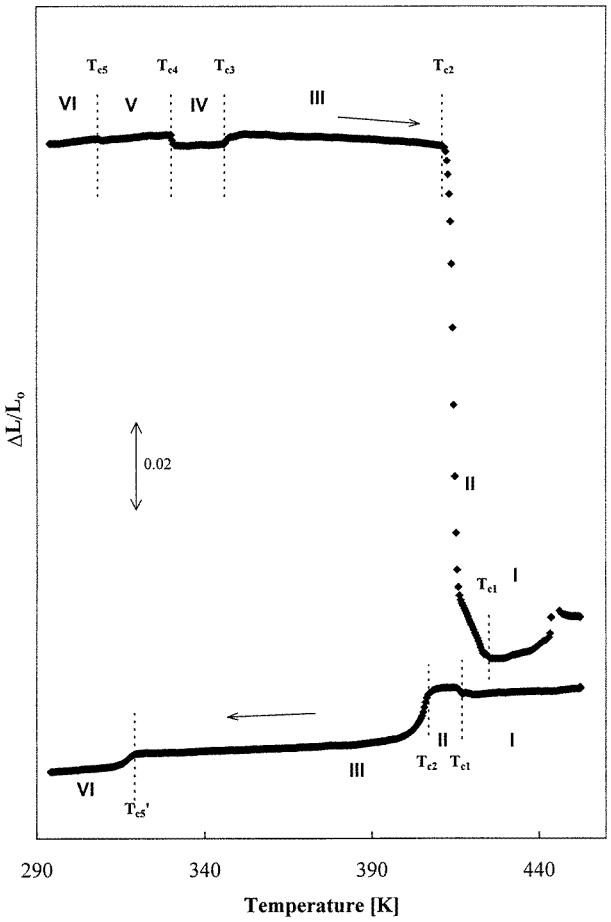

Figure 6. Temperature dependence of the linear thermal expansion, $\Delta L/L_0$, measured along the c-axis on cooling and heating at a rate of 1 K min^{-1} for $[C(NH_2)_3]_3Bi_2Br_9$.

unit cell and consequently will not contribute to the value of electric permittivity. In the GBB crystals the phase transitions at T_{c5}, T_{c4} and T_{c3} are accompanied by small changes in epsilon (ε_b') values. In our opinion these dielectric anomalies may be connected with the changes in the anionic sublattice. The anionic sublattice is composed of isolated bioctahedral $Bi_2Br_9^{3-}$ units sharing faces. In phase VI these units are ordered and not significantly distorted. We cannot expect further distortion on increasing temperature in subsequent high temperature phases. Changes in electric permittivity are, therefore, most probably connected with increase of disorder of $Bi_2Br_9^{3-}$ units. Taking into account the shape of bioctahedral anionic units we would expect onset of reorientations around line joining Bi atoms (the axis of the smallest moment of inertia).

3.5. Birefringence measurements and optical observations

The virgin samples of GBB are typically of single domain type. They have preferred cleavage plane perpendicular to the monoclinic axis b. During the preparation of samples for optical measurements (cutting and cleaving) most easily are introduced domains with walls parallel

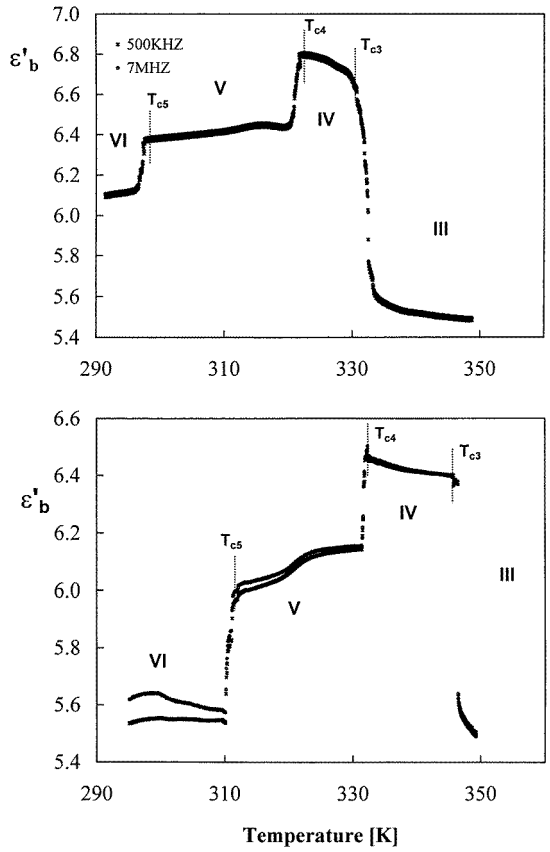

Figure 7. Temperature dependence of the real part of the complex electric permittivity measured along the *b*-axis on cooling (upper part) and on heating (lower part) of the $[C(NH_2)_3]_3Bi_2Br_9$ crystals heated up to 350 K (phase (III)).

to the $(10\bar{1})$ plane. By applying stronger stress, domains with walls along (101) (001) and (100) are also obtained relatively easily. The symmetry analysis [21, 23] suggests tetragonal symmetry of the parent phase.

The orientations of optical indicatrix axes show strong dispersion. The angle ϕ between the long axis of the indicatrix and the *c*-axis equals 15° for red light while for blue it is 24°. The value Δn_b at room temperature is equal to 0.02.

On heating, at $\sim$308 K there is a jump of the birefringence by 0.004 (see figure 9), oblique dispersion of the optical axes vanishes and the orientation of the indicatrix changes ($\phi = 7^\circ$) on transformation to a new phase. Lack of changes in the ferroelastic domain pattern suggests that crystal remains monoclinic. Thermal hysteresis for this transition depends on thermal history of the sample and varies from 3 to 12 K.

On further heating after non-monotonic increase of the birefringence at $\sim$333 K there is a next jump of Δn_b and resulting change in the orientation of the optical indicatrix; its axes are now nearly parallel to the monoclinic axes *a* and *c* ($\phi = -4^\circ$).

Reaching 347 K we observe a jumpwise decrease of the birefringence, disappearance of existing domain walls and a new position of the indicatrix axes—now in the diagonal (with respect to the room temperature monoclinic axes) position (figures 10(a) and 10(b)). It may

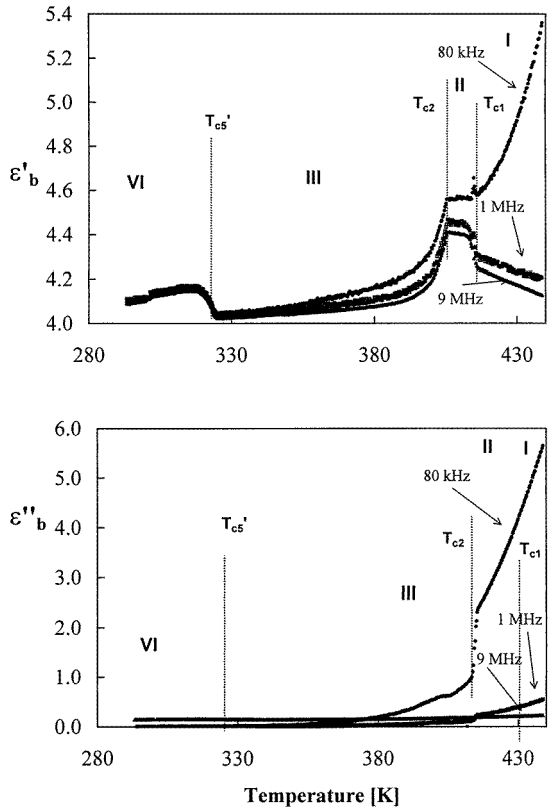

Figure 8. Temperature dependence of the real part (upper part) and imaginary part (lower part) of the complex electric permittivity measured along the *b*-axes on cooling of the $[C(NH_2)_3]_3Bi_2Br_9$ crystals heated up to phase (I).

be interpreted as a result of ferroelastic phase transition to the orthorhombic (because of the unique character of the *b*-axis) system with the *a*- and *c*-axes turned about 45° with respect to the monoclinic ones which is confirmed by the x-ray temperature studies.

On further heating birefringence decreases and at 413 K we observe the next phase transition (IV to III), which results in formation of a very fine and complex domain structure accompanied by cracks and strains (figure 11). Small sizes of domains and strains do not allow us to analyse the resulting twinning. The thermal hysteresis of this transition is below 1 K. At 416–417 K we observe rebuilding of the domain structure which may be a result of the next phase transition.

At 425 K crystal transforms to the phase optically isotropic. From the observed domain patterns and unique character of the *b*-axis, we conclude that in the high temperature phase (I) the crystal belongs to the tetragonal system. The phase front seems to be a little diffused, probably from the character of the existing domain structure (figure 12). The observed thermal hysteresis is about 1.5 K.

Since the phase transition at 413 K was particularly destructive for our crystal (see figure 13), we were unable to carry similar observations during cooling of the sample after reaching the I or II phases. We completed several studies of phase transitions of this crystal involving cycles below 400 K. The thermal hysteresis for the III to IV phase transition is especially large. On heating it takes place at 347 K, whereas on cooling at 333 K. Below

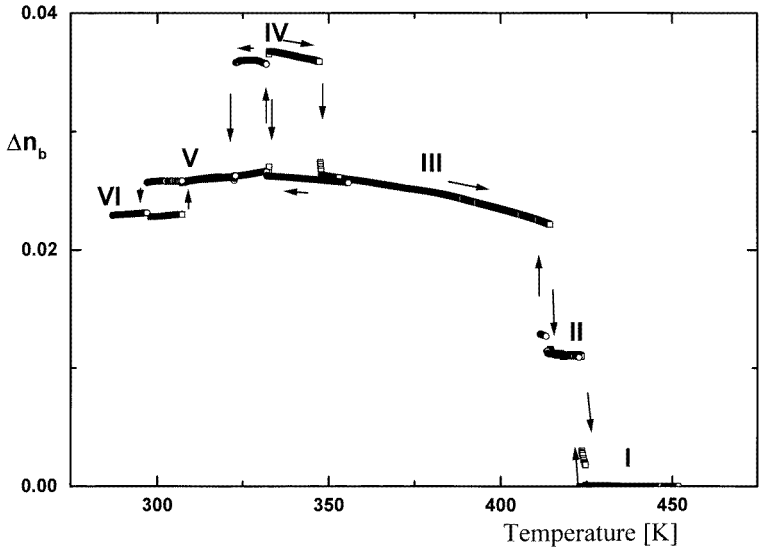

Figure 9. The collected results of linear birefringence measurements in the $[C(NH_2)_3]_3Bi_2Br_9$ crystals. Circles—data obtained on cooling and squares—on heating (cooling/heating rate of 0.5 K min^{-1}).

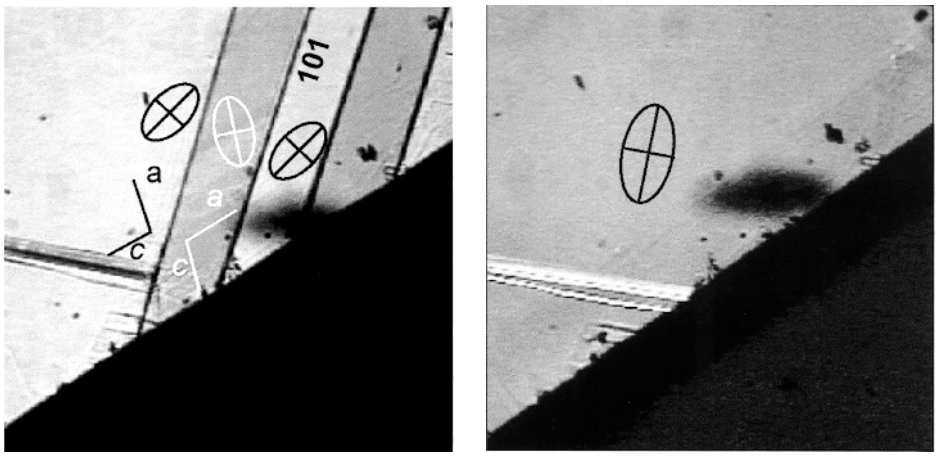

(a) (b)

Figure 10. (a) Ferroelastic domain structure of GBB crystal at room temperature (phase VI, after cooling from phase III). (b) The same area of the crystal in phase III. The new position of the indicatrix is marked.

333 K the domain structure with walls along (101) is formed in contrast to the initial domain structure where walls along $(10\bar{1})$ are prevalent. It is possible to observe coexistence of phases III and IV with the interface oriented very near domain walls in the phase IV (figure 14) in agreement with predictions of model of strain free interface between the parent and daughter phases [22, 23].

On further cooling we recorded two jumpwise transitions at 323 and 300 K. The phase below 300 K has optical properties identical to the initial (virgin crystal) one.

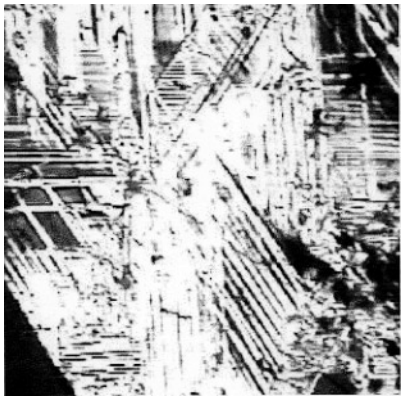

Figure 11. Ferroelastic domain structure after the phase transition at 413 K (on heating).

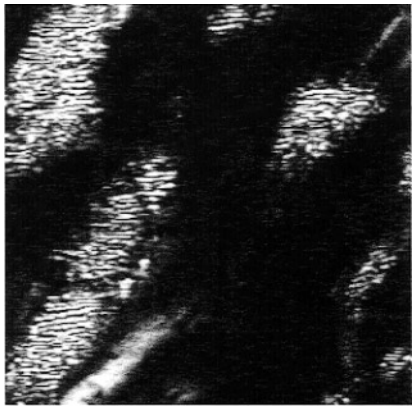

Figure 12. Transformation of the $[C(NH_2)_3]_3Bi_2Br_9$ crystal to the parent phase (I) at 425 K.

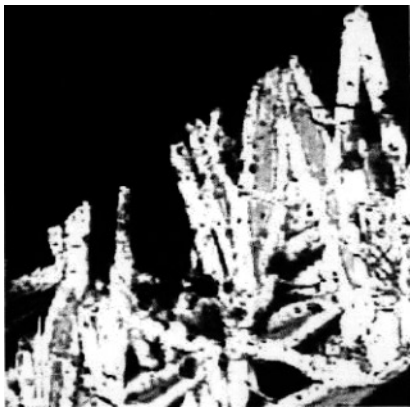

Figure 13. Ferroelastic domain pattern of the $[C(NH_2)_3]_3Bi_2Br_9$ crystal just after reaching phase II (starting from parent phase I).

Applied optical methods allow us to distinguish six phases of the GBB crystal and five transitions—all of them first order type—and point to the probable symmetries of these phases.

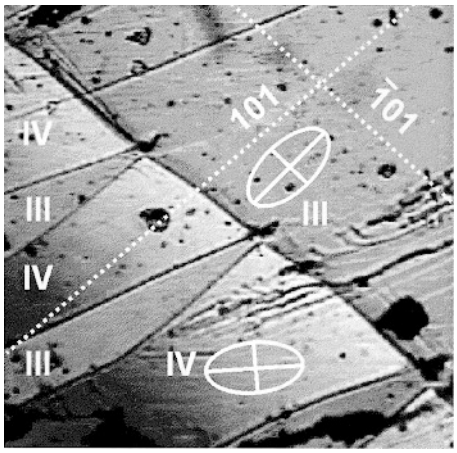

Figure 14. The phase front between phases III and IV (334 K, on cooling).

4. Summary

X-ray diffraction studies showed that the structure of the $[C(NH_2)_3]_3Bi_2Br_9$ crystal at room temperature consists of isolated bioctahedral $Bi_2Br_9^{3-}$ units and ordered guanidinium cations. The compound crystallizes in the monoclinic symmetry with the space group $P2_1/m$.

The structural phase transitions in GBB were investigated using dielectric permittivity, differential scanning calorimetry, dilatometric, birefringence and optical observations. Six phases were identified by these techniques. All structural phase transitions were found to be strongly of first order; at 311 K, 333.5 K, 350 K, 415 K and 425 K. The values of the transition entropies suggest that most of the phase transitions in GBB are of the order–disorder type. The optical observation showed that the ferroelastic domain structure is maintained between the room temperature phase and 425 K. The paraelastic parent phase is suggested to have the tetragonal symmetry.

Acknowledgment

This work was supported by the Polish State Committee for Scientific Research (project register No 3T09A 093 10).

References

[1] Jakubas R and Sobczyk L 1990 *Phase Transitions* **20** 163
[2] Sobczyk L, Jakubas R and Zaleski J 1997 *Pol. J. Chem.* **71** 265
[3] Varma V, Bhattacharjee R, Vasan H N and Rao C N R 1992 *Spectrochim. Acta* A **48** 1631
[4] Ishihara H, Watanabe K, Iwata A, Yamada K, Kinishita Y, Okuda T, Krishnan V G, Dou S and Weiss A 1992 *Z. Naturf.* a **47** 65
[5] Kozioł P, Furukawa Y and Nakamura D 1991 *J. Phys. Soc. Japan* **60** 3850
[6] Rajan P K, Jagadeesh B, Venu K and Sastry V S S 1996 *Solid State Commun.* **10** 535
[7] Jakubas R, Krzewska U, Bator G and Sobczyk L 1988 *Ferroelectrics* **77** 129
[8] Jakubas R 1986 *Solid State Commun.* **60** 389
[9] Jakubas R, Sobczyk L and Matuszewski J 1987 *Ferroelectrics* **74** 339
[10] Jakubas R, Czapla Z, Galewski Z and Sobczyk L 1986 *Ferroelectr. Lett.* **5** 143
[11] Mróz J and Jakubas R 1994 *Ferroelectr. Lett.* **17** 73
[12] Iwata M and Ishibashi Y 1992 *Ferroelectrics* **135** 283

[13] Miniewicz A, Jakubas R and Ecolivet C 1990 *Ferroelectrics* **106** 249
[14] Kosturek B, Przesławski J and Jakubas R 1990 *Solid State Commun.* **75** 673
[15] Zaleski J, Jakubas R and Sobczyk L 1990 *Phase Transitions* **27** 25
[16] Kuok M H, Ng S G, Tun L S, Rang Z L, Iwata M and Ishibashi Y 1998 *Solid State Commun.* **108** 159
[17] Iwata M, Eguchi M, Ishibashi Y, Sasoki S, Shimizu H, Kawai T and Shimanuki S 1993 *J. Phys. Soc. Japan* **62** 3315
[18] Wood I G and Glazer A M 1980 *J. Appl. Crystallogr.* **13** 224
[19] Ehringhaus A E 1939 *Z. Kristallogr.* A **102** 85
[20] Sheldrick G M SHELXl97 program for the refinement of crystal structures, University of Göttingen
[21] Sapriel J 1975 *Phys. Rev.* B **12** 5128
[22] Boulesteix C, Yangui B, Ben Salem M, Manolikas C and Amelinckx S 1986 *J. Physique* **47** 461
[23] Dudnik E F and Shuvalov L A 1989 *Ferroelectrics* **98** 207